Electronic Supplementary Material (ESI) for Journal of Materials Chemistry A.

Supplementary Information

Tailoring the Supramolecular Interaction of Ionic Liquids for High-Sensitivity Temperature Monitoring Under High Pressure

*Beihang Xu, Yao An, Xinjia Zheng, Zhiwu Chen, Zhaoxiang Yang, Yongjia Yang, An Zhang, Yapei Wang, and Yonglin He**

1. Experimental Section

1.1 Materials:

1-Butyl-3-methylimidazolium dicyanamide ([BMIm][N(CN)]$_2$) was purchased from Lanzhou Greenchem ILS, LIPC, CAS (Lanzhou, China). Iron(III) chloride ($FeCl_3$) was purchased from Meryer (Shanghai) Chemical Technology Co., Ltd..

1.2 Instruments and characterizations:

^{1}H NMR spectra were recorded on a Bruker AVANCE 600 MHz spectrometer in $CDCl_3$. Resistance responses were measured by using a CHI760e electrochemical workstation (Shanghai CH Instrument Co., Ltd.). The temperature control was achieved using Peltier modules. Thermal responses were measured by UT 325 digital thermometers (UNI-T Technology (China) Co., Ltd.). The density and viscosity of solutions involved in this study were measured by density meter (DMA 4500 M, Anton Paar) and microviscometer (Lovis 2000 ME, Anton Paar), respectively. Differential scanning calorimetry (DSC) curves were recorded on a TA instrument Discovery 250 system with a flow N_2 rate of 50 mL/min. The samples (about 20 mg) were first heated to 80 °C and kept for 5 min. Heating cycles from -20 °C to 80 °C were measured with the heating or cooling rate of 10 °C/min. To eliminate the thermal history, data from the second heating cycle were used. The variable-temperature FTIR spectra were obtained through a CaF_2 optical window, with a Bruker TENSOR 27. The pressure resistance performance of the temperature sensor was characterized by an Instron LEGEND 2367 apparatus using a compression mode. The temperature sensor's resistance rate change was evaluated with the aid of a dynamic mechanical analyzer (TA Discovery 850) in an arranged temperature range at a heating and cooling rate of 2°C/min within the range of 20 °C to 50 °C. Thermal images were taken by IR-384 thermal infrared imager (RNO).

1.3 Density functional theory (DFT) calculations:

The density functional theory (DFT) calculations were carried out with the Gaussian 09W software package to optimize the structure of molecules. Geometrical optimization adopted the pbe1pbe method with 6-31G(d) basis sets (for C, N, H) and SDD basis sets (for Fe^{3+}). The electronic density analysis and interaction region indicator (IRI) analysis were performed using Multiwfn version 3.8 (dev) and VMD 1.9.3 software.

2. Supplementary Discussion

2.1 Vogel-Tammann-Fulcher equation:

The conductivity as a function of temperature, fits extremely well into the Vogel-Tammann-Fulcher equation:

$$\boldsymbol{\sigma(T) = \sigma_{\infty} exp\left(\frac{-B}{T - T_v}\right)} \quad (\boldsymbol{S1})$$

Where parameters including $\boldsymbol{\sigma_{\infty}}$, $\boldsymbol{B}$, and $\boldsymbol{T_v}$ are constants for a certain doped ionic liquid.

2.2 Thermal response equation:

The relationship between conductivity change and temperature change:

$$\boldsymbol{\frac{\Delta G}{G_0} = exp\left[\frac{B(T - T_0)}{(T_0 - T_v)(T - T_0 + T_0 - T_v)}\right] - 1} \quad (\boldsymbol{S2})$$

2.3 Modified Nernst-Einstein equation:

The molar conductivity ($\boldsymbol{\Lambda}$) of an ionic liquid can be described using the modified Nernst-Einstein equation:

$$\boldsymbol{\Lambda = \frac{1}{k_B T} \sum_i \gamma_i q_i^2 D_i} \quad (\boldsymbol{S3})$$

where $\boldsymbol{k_B}$ is the Boltzmann constant, $\boldsymbol{T}$ is the temperature, $\boldsymbol{\gamma_i}$ is the fraction of cations or anions in the free state, $\boldsymbol{q_i}$ is the charge number of the corresponding ion and $\boldsymbol{D_i}$ is its diffusion coefficient.

2.4 The relationship between conductivity (σ) and viscosity (η):

According to the combination of the Einstein relation (eq. S4) for the relationship between the diffusion coefficient ($\boldsymbol{D}$) in a liquid and its carrier mobility ($\boldsymbol{u}$), and the Stokes-Einstein equation (eq. S5) for the relationship between the diffusion coefficient ($\boldsymbol{D}$) in a liquid and its dynamic viscosity ($\boldsymbol{\eta}$), the conductivity ($\boldsymbol{\sigma}$) can be numerically connected with the viscosity ($\boldsymbol{\eta}$) (eq. S6):

$$\boldsymbol{D = \frac{k_B T}{zq} \times u} \quad (\boldsymbol{S4})$$

$$\boldsymbol{D = \frac{k_B T}{6\pi\eta r}} \quad (\boldsymbol{S5})$$

$$\sigma = nzq \times u = \frac{nz^2q^2}{6\pi\eta r} \quad (S6)$$

where k_B is the Boltzmann constant, z is the number of charges carried by the carriers, q is the single-electron charge and r is the radius of the ions. Therefore conductivity (σ) is inversely proportional to the viscosity (η) of the conducting medium, which is also the empirical Walden rule.

So the conductivity (σ) can be expressed as follows:

$$\sigma = \frac{A}{\eta_\infty} exp\left(-\frac{E_a}{RT}\right) \quad (S7)$$

where A is the constant for a specific ionic liquid.

2.5 Calculation of enthalpy, entropy, and Gibbs energy changes:

The heat capacity can be expressed from its definition equation in the form:

$$C_{p,m} = \frac{1}{n}\left(\frac{\partial H}{\partial T}\right)_p = \frac{1}{n}\left(\frac{\frac{\partial H}{\partial t}}{\frac{\partial T}{\partial t}}\right)_p = \frac{HF}{n \times \beta} \quad (S8)$$

where n is the molar amount of the ionic liquid, H is the enthalpy, T is the temperature, t is the time, HF (W) is the heat flow, and B (°C/min) is the heating or cooling rate. Eq. S8 is derived using the equilibrium thermodynamics definition of heat capacity.

Based on the heat capacities, it is possible to calculate enthalpy, entropy, and Gibbs energy changes of ionic liquids over a temperature range from 293.15 to 333.15 K.

$$\Delta H = \int_{293.15K}^{333.15K} C_p dT \quad (S9)$$

$$\Delta S = \int_{293.15K}^{333.15K} (C_p/T) dT \quad (S10)$$

$$\Delta G = \Delta H - T\Delta S \quad (S11)$$

2.6 Interaction region indicator (IRI):

The IRI function is defined as follows:

$$IRI(r) = \frac{|\nabla\rho(r)|}{[\rho(r)]^a} \quad (S12)$$

where a is a tunable parameter, and the standard definition of IRI employs a value of a=1.0. IRI is essentially the gradient norm of electron density weighted by scaled electron density. $sign(\lambda_2)\rho$ function is then mapped with different colors onto the isosurfaces of IRI, vividly depicting the nature of the interaction regions revealed by IRI. The $sign(\lambda_2)$ represents the

sign of the second-largest eigenvalue of the Hessian matrix of the electron density, providing a certain ability to differentiate attractive and repulsive interactions. Regions with relatively high $\boldsymbol{\rho}$ values and consequently larger $\boldsymbol{sign(\lambda_2)\rho}$ values indicate relatively strong interactions, whereas regions with lower $\boldsymbol{\rho}$ values and consequently smaller $\boldsymbol{sign(\lambda_2)\rho}$ values do not exhibit significant interactions, or any interactions observed can be attributed, at most, to very weak interatomic vdW interactions.

3. Supplementary Figures

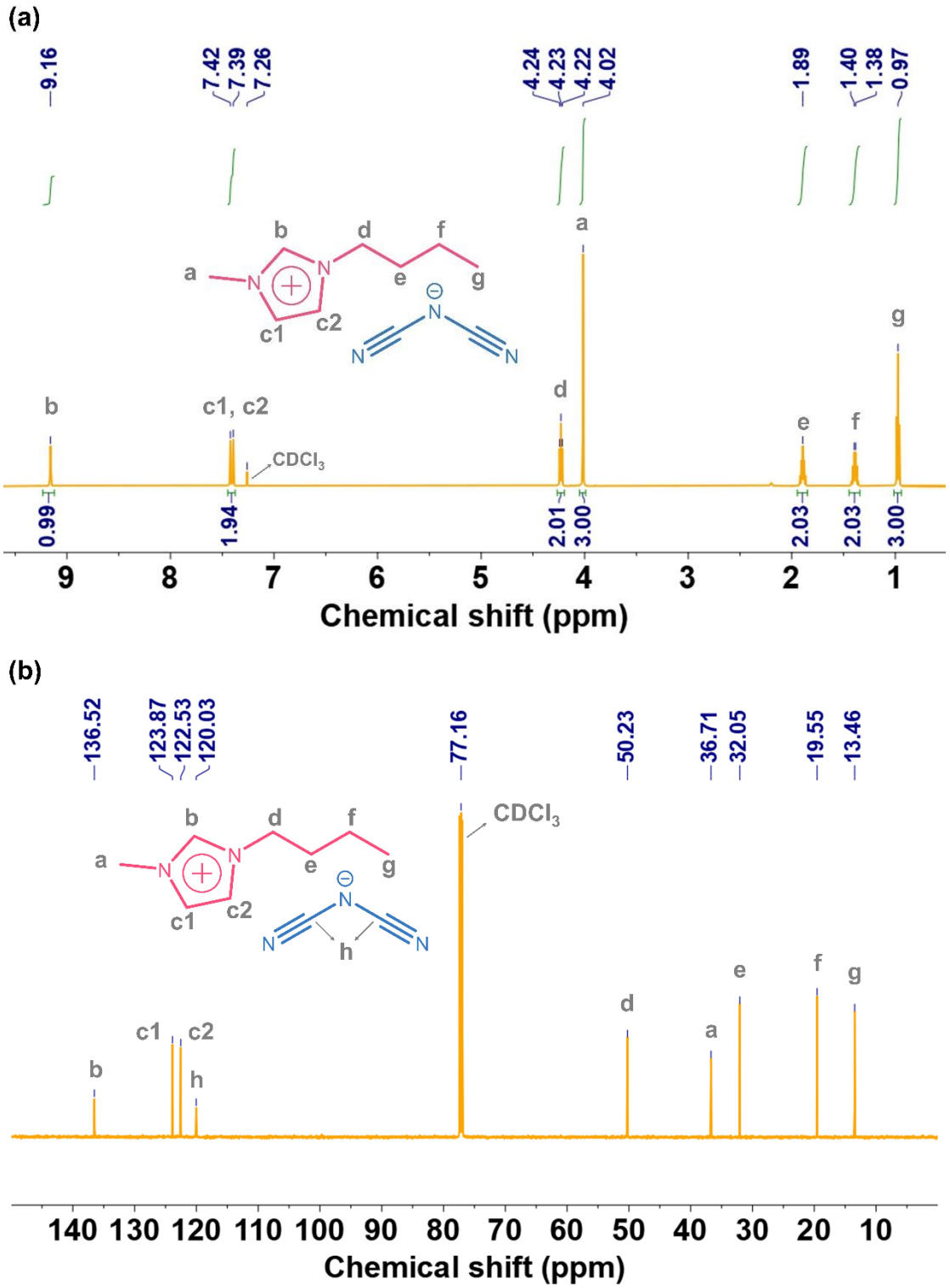

Fig. S1. (a) ^{1}H NMR and (b) ^{13}C NMR spectra of [BMIm][N(CN)$_2$] in CDCl$_3$.

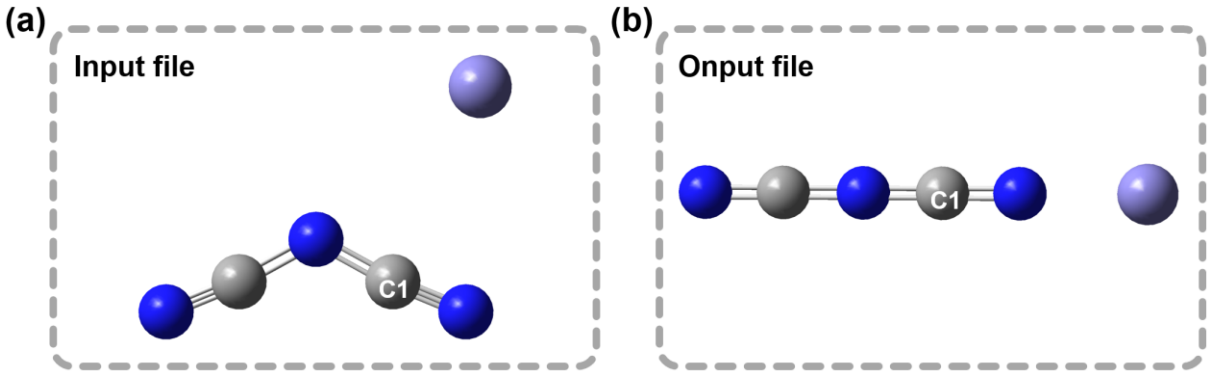

Fig. S2. Input (a) and output (b) files for the potential energy surface scan using the C1 atom of $[N(CN)_2]^-$.

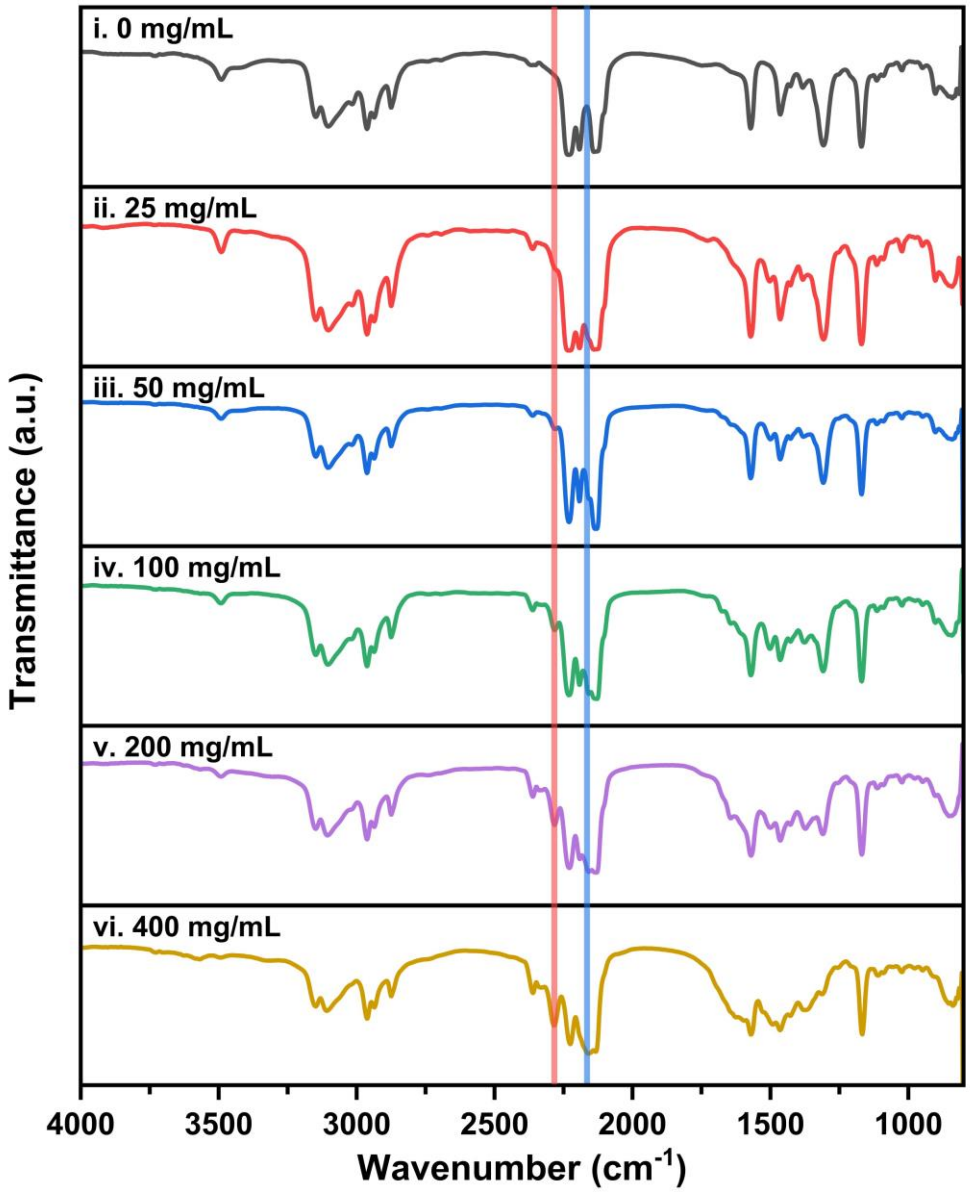

Fig. S3. FTIR spectra of ionic liquids containing 0, 25, 50, 100, 200, and 400 mg/mL FeCl3, respectively.

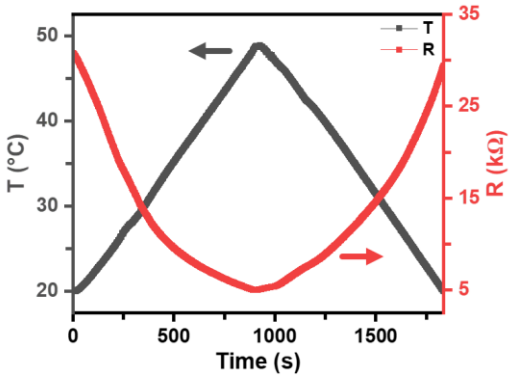

Fig. S4. The resistance response rate at the same heating and cooling rate within the temperature range of 20 to 50 °C.

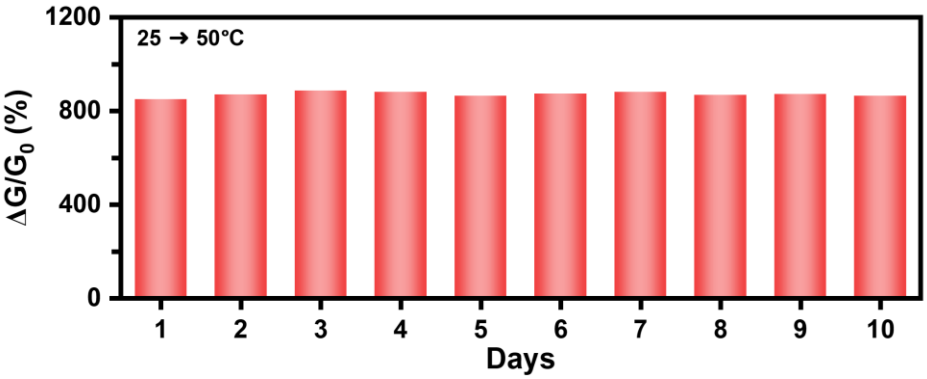

Fig. S5. Long-term stability of the thermal response of the temperature sensor between 25 and 50 °C.

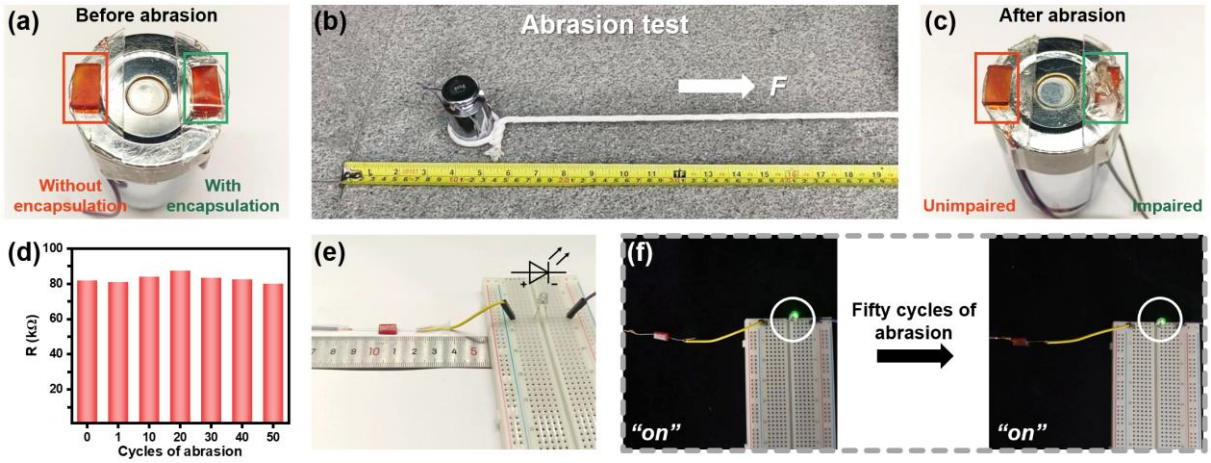

Fig. S6. Wear Resistance of Temperature Sensors. (a) The weight carrying with temperature sensors before abrasion. (b) Optical images of the abrasion test. (c) The weight carrying with temperature sensors after abrasion. (d) Resistance values of the unencapsulated temperature sensor after abrasion. (e) Circuit constructed with the temperature sensor connected to light-emitting diodes. (f) Light-emitting diodes lighted before and after friction.

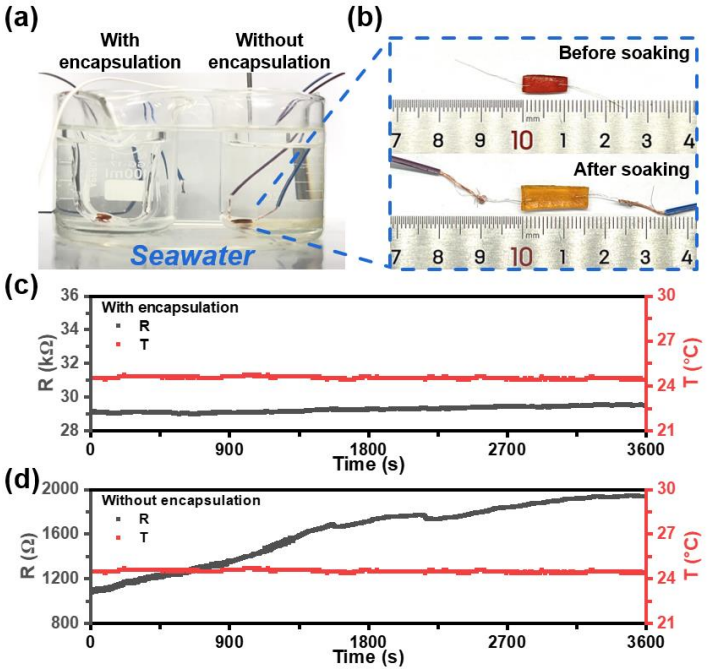

Fig. S7. The influence of seawater on temperature sensors. (a) Optical image of the experiment illustrating the impact of seawater on the temperature sensor. (b) Optical images of the unencapsulated temperature sensor before immersion in seawater and after one hour of immersion. (c-d) Continuous and synchronous time evolution curves of temperature (red curve) and resistance (black curve) recorded by the encapsulated temperature sensor (c) and the unencapsulated temperature sensor (d).

Fig. S8. Optical images of (a) the polyurethane swelled by ionic liquid and (b) the ionic liquid-based temperature sensor used in automotive loading experiments.

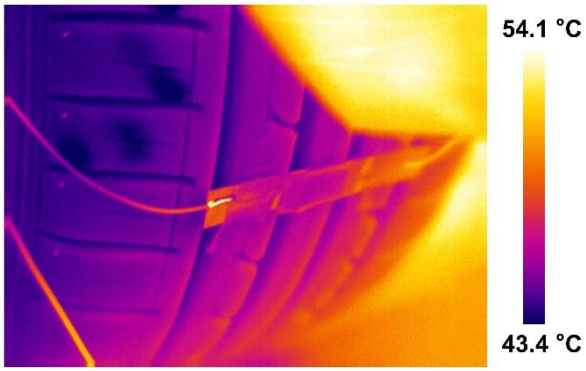

Fig. S9. Infrared photo of automotive loading experiment.

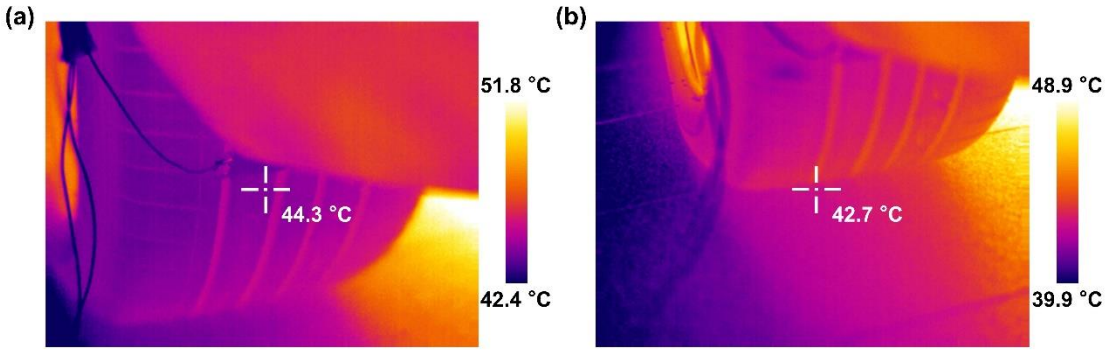

Fig. S10. Infrared photos of the tire (a) and the ground (b).

4. Supplementary Movie

Movie S1. Temperature detection under high pressure.